Morphology of TiO_2 Nanoparticles as Fingerprint for the Transient Absorption Spectra: Implications for Photocatalysis

Ángel Morales-García*, Rosendo Valero and Francesc Illas

Departament de Ciència de Materials i Química Física & Institut de Química Teòrica i Computacional (IQTCUB), Universitat de Barcelona. c/ Martí i Franquès 1-11, 08028 Barcelona, Spain

Abstract

Understanding the relationship between structural properties and the character of the charged carriers in photoactive TiO_2 nanoparticles is fundamental to improve their photocatalytic activity. Transient Absorption Spectroscopy (TAS) is often used to explore the character of charge carriers but carrying out experiments on well-defined nanoparticles with a given morphology and selected size is extremely difficult. Here, hybrid time-dependent density functional theory (TDDFT) based calculations carried out for realistic TiO_2 nanoparticles (NPs) with bipyramidal, truncated and spherical morphologies reveal that electron trapped carriers are quite sensitive to the NP morphology. In particular, these carriers are shallowly trapped in faceted NP whereas they are deeply trapped in those exhibiting a spherical morphology. In addition, the simulated absorption spectra can be compared directly to experimental ones obtained by TAS thus allowing to provide additional information regarding the morphology of TiO_2 NPs in a given sample. Note that, although the present study focuses on TiO_2 nanoparticles, it can be easily extended to other photoactive materials such as ZnO or WO_3 NPs thus allowing to extract information regarding the relationship between NP morphology and the nature of the low lying excited states.

INTRODUCTION

Semiconductor-based photocatalysts have been the subject of numerous multi- and interdisciplinary studies since the discovery of water splitting through the so-called Honda-Fujishima effect.[1] These materials are involved in a broad variety of important applications, including self-cleaning surfaces, air and water purification systems, sterilization, hydrogen evolution, photoelectrochemical conversion and, obviously, water splitting.[2-4] Among the large number of semiconductor materials investigated for photocatalytic applications, titanium dioxide (TiO_2) continues to be the workhorse in the field because of its low cost and high stability.[5-7] It is generally accepted that the photocatalytic mechanism involved on powdered semiconductor materials implies a complex sequence of five photophysical and electrocatalytic processes: (*i*) photon adsorption, (*ii*) exciton separation, (*iii*) charge carrier diffusion and transport, (*iv*) catalytic efficiency and, finally, (*v*) mass transfer of reactants and products.[8] This five-gear concept needs to be perfectly engrained to lead to optimal quantum yield that leads to, for instance, a high solar-to-hydrogen conversion efficiency for the particular case of photocatalytic water splitting process.

The efficiency of a photocatalytic reaction can be determined by analyzing the reactivity of the photogenerated electrons (e^-) and holes (h^+) with molecules at the photocatalyst surface. Experimentally, transient absorption spectroscopy (TAS) emerges as one of the most powerful techniques, due to its high temporal resolution (~100 fs) and its capability to identify transient chemical species.[9] Earlier electron-hole dynamics studies involving this technique have been carried out on colloidal TiO_2 nanoparticles (NPs) samples, extending the range of absorption spectra of either e^- and h^+ from the UV to the IR region.[10] To avoid the trapped e^- and h^+ overlapping in the VIS region, these experiments were performed in the presence of e^- or h^+ scavengers. In this way, the trapped e^- and h^+ are located at longer (~700 nm) and shorter (~500 nm) wavelengths, respectively.[11] Although the assignment of TAS observed transitions to individual electronic excited states is quite difficult, it is possible to distinguish the carriers from the position and shape of the trapped carriers related bands. Interestingly, the nature of a charge carrier is identified by the position of the band at high (or low) energy excitations corresponding to deep (or shallow) trapped charge carriers. In addition, a narrow-shaped band is associated to a charge carrier with a locally trapped character, whereas the broad-shaped one indicates a larger delocalization.

It is well known that the morphology of the semiconductor-based photocatalyst has direct implications in electronic structure and related properties and, consequently, in the photocatalytic performance.[12] From an experimental point of view, it is not easy to distinguish properly between size and shape effects. Fortunately, for different types of TiO_2 materials —polymorphs, surfaces, and nanoparticles— computational modeling provides an unbiased way to analyze the morphology effect for a given composition and the composition effect for a given morphology.[13-19] Indeed, it has been experimentally shown that the atomic structure critically affects the nature of the photogenerated carriers.[20,21] In particular, a detailed kinetic study of the e^-–h^+ recombination, based on TAS measurements, reports that anatase-derived photocatalysts are ~30 times more reactive than their rutile-derived counterparts.[20] This large difference is due to the location of the

photogenerated electrons, which are deeply trapped in rutile and, thus, the reactivity is lower than that of free or shallowly trapped electrons generated in anatase-derived photocatalysts. Despite the important role that photogenerated species have in photocatalytic processes, simulations on the absorption spectra of photoactive materials are scarce.[22-24] Therefore, computational spectroscopy studies of photogenerated carriers in realistic photoactive NPs appear as necessary. In this way, Nunzi *et al*.[25] recently investigated the absorption spectra of photogenerated charge carriers in a prototypical anatase $(TiO_2)_{38}$ NP by using time dependent density functional theory (TDDFT) based calculations. While this is an interesting study, the fact that involves just one NP does not permit to extract conclusions regarding the effect of the NP morphology on the absorption spectra. To provide this information is the main goal of the present study. To this end, three stoichiometric $(TiO_2)_n$ anatase-derived NPs with different morphology are studied (Figure 1). These NPs have been designed through a top-down protocol,[17] and involve a bypiramidal truncated $(TiO_2)_{29}$, a bypiramidal $(TiO_2)_{35}$ and a spherical-like $(TiO_2)_{43}$ nanoparticle.

COMPUTATIONAL DETAILS

State-of-the-art hybrid DFT and TDDFT based calculations are used to simulate the corresponding TAS spectra as implemented in TURBOMOLE v7.3 electronic structure package.[26] The PBE0 hybrid density functional along with the 6-31G* People basis set are selected for all DFT and TDDFT calculations. The mid-size m3 quadrature grids were used for the integration of the exchange-correlation functional.[27,28] For reasons of computational efficiency, the resolution of identity (RI)[29,30,31-32] approximation is employed for the evaluation of two-electron integrals. In this approximation, auxiliary basis sets need to be introduced. Thus, the 6-31G* auxiliary basis set is used for oxygen, and a universal auxiliary basis set is used for titanium, as a 6-31G* auxiliary basis is not defined for this atom. The protocol follows (*i*) the neutral spin-singlet ground state NPs geometries are optimized at the PBE0/6-31G* level, then, (*ii*) for the cationic and anionic spin-doublet NPs (i.e., with the h^+ and e^- unrelaxed polarons) at their optimal ground-state geometries, the lowest 100 singlet TDDFT excitations are computed. Subsequently, the cationic and anionic NPs were also geometrically relaxed, and the lowest 100 singlet TDDFT excitations were also computed at the relaxed geometries. We want to point out that TDDFT is chosen since, for the rather large size systems studied in the present work, it is surely the most suitable method to approach excited states; the choice of PBE0 hybrid density functional is justified from previous work showing that these are appropriate to properly describe the self-trapping of charge carriers in TiO_2 NPs.[33] The absorption spectra of the h^+ and e^- relaxed polarons are calculated by choosing the dipole length gauge for the transition dipole moments and broadening all the computed excitation peaks with a Gaussian function of 0.16 eV width, and plotting the sum of the broadened peaks with the SpecDis[34] software. Also, the sum of the h^+ and e^- spectra is included in the plots. The electronic density of the most relevant MOs participating in the electronic excitations was extracted as standard *cube* files and was plotted with the Jmol[35] software.

Following this methodology, we analyze the properties of single photogenerated e^- and h^+ species by considering the unrelaxed and relaxed negatively and positively charged $(TiO_2)_n$ (n = 29, 35, and 43) NPs. Finally, TDDFT calculations with the PBE0 functional have been carried out to simulate the absorption spectra of the fully relaxed $(TiO_2)_n^-$ and $(TiO_2)_n^+$ NPs. The obtained results allow one to access the simulated TAS spectra, providing insights into the nature of excited states[25] and, more important, the sensitivity of TAS spectra to the nanoparticle morphology.

RESULTS AND DISCUSSION

We start the discussion of the results with a detailed analysis of the PBE0 Kohn-Sham energy levels depicted in Figure 2 that correspond to the equilibrium geometry of the neutral $(TiO_2)_n$ (n = 29, 35, and 43) NPs and of the charged $(TiO_2)_n^-$ and $(TiO_2)_n^+$ NPs in both the unrelaxed and relaxed geometry. The HOMO-LUMO gaps of neutral NPs (the so-called optical gap, O_{gap})[36] are 5.01, 5.16, and 3.77 eV for the bipyramidal, truncated, and spherical morphologies, respectively. This result is in agreement with previous work on TiO_2 NPs[17] showing that the quantum confinement due to the nanoparticle size leads to an energy gap above the calculated band gap for bulk anatase using the same functional and also above the experimental observation in the bulk anatase. In addition, the nanoparticle morphology has, as expected, a clear effect on the O_{gap}, which is lower in the spherical NPs than in the faceted ones, also in agreement with recent work.[19] Further interesting results are found in the changes of the Kohn-Sham energy levels upon the addition of e^- and h^+. For the negatively and positively charged TiO_2 NPs, the e^- and h^+ states correspond respectively to adding one electron to the neutral ground state LUMO or removing one electron from the neutral ground state HOMO. The resulting singly occupied orbital is usually referred to as SOMO. In a spin restricted description, the two spinorbitals corresponding to the spatial SOMO are degenerate. However, in a spin unrestricted formalism these are no longer degenerate, the occupied/unoccupied spinorbital is referred to as SOMO/SUMO. This is the notation used in the present work.

For the negatively charged $(TiO_2)_{35}^-$, $(TiO_2)_{29}^-$, and $(TiO_2)_{43}^-$ NPs at the neutral ground state geometry, the spinorbital of interest is the SOMO, that is systematically located below LUMO by 0.75, 0.88, and 0.54 eV, respectively. Similarly, for the positively charged $(TiO_2)_{29}^+$, and $(TiO_2)_{35}^+$ and $(TiO_2)_{43}^+$, the spinorbital of interest is the SUMO corresponding to the hole state. For these NPs, the SUMO is found above HOMO by 0.48, 0.33 and 0.33 eV. After geometry optimization for the negatively and positively charged NPs, SUMO and SOMO spinorbitals exhibit significant shifts. Thus, for $(TiO_2)_{35}^-$, $(TiO_2)_{29}^-$, and $(TiO_2)_{43}^-$, the SOMO is now located below LUMO by 1.85, 2.46, and 2.62 eV whereas for $(TiO_2)_{35}^+$, $(TiO_2)_{29}^+$, and $(TiO_2)_{43}^+$ the SUMO appears above HOMO by 3.79, 3.45, and 3.54 eV, respectively. The present trends are in good agreement with those reported in a previous study for the $(TiO_2)_{38}$ NP.[25] Interestingly, the SUMO upshifts are very similar for all TiO_2 NPs. This observation is related to a similar localization of the hole state regardless of nanoparticle morphology. On the other hand, we found that the SOMO downshifts increase moving from bipyramidal towards spherical morphology, yielding the largest localization of the electron state in the

spherical NP. In contrast to these different tendencies observed in the localization of electron states, the hole state is more localized than the electron state for all investigated TiO_2 NPs (Figure 1). The electron densities for unrelaxed and relaxed states corresponding to SUMOs and SOMOs, depicted in Figure S1, show that the structural relaxation induces the localization.[25]

The computed absorption spectra of the $(TiO_2)_n^-$ and $(TiO_2)_n^+$ (n = 29, 35, and 43) NPs in their relaxed geometries are presented in Figure 3. Note that the first hundred excitations are considered to build the spectra, as explained in the SI. Since the simulated spectra can be directly compared to experimental TAS ones,[37,38] a detailed discussion follows by analyzing the peak positions and spectral shapes. Starting with the bipyramidal $(TiO_2)_{35}$ NP, trapped electrons have a broad band in the 340–1500 nm range with a maximum at ca. 720 nm, whereas trapped holes have a narrower band (ca. 260–460 nm) with the absorption maximum at ca. ~380 nm. On the other hand, for the truncated $(TiO_2)_{29}$ NP, the trapped electron band is broader than that of the trapped hole, ca. 270–1100 nm and ca. 260–580 nm, respectively. Note that the trapped electron band has two maximum peaks at ca. 280 and ca. 500 nm, whereas the trapped hole band exposes maxima at ca. 700 and 860 nm. Finally, the spherical $(TiO_2)_{43}$ NP shows rather different spectra with similar wavelengths for the bands of both trapped electron and hole. Note that here the maximum peak positions are observed at ca. 300 and 380 nm for the trapped electron and hole, respectively. In general, the position of the trapped hole bands is almost the same for all titania nanoparticles regardless of morphology. However, the band position of the trapped electrons shifts towards lower wavelengths when moving towards spherical morphology, inducing a hypsochromic effect. This evolution clearly indicates that electrons are shallowly trapped in the bipyramidal NP, whereas they are deeply trapped in the spherical one. On the other hand, the $(TiO_2)_{35}$ faceted NP bears a SOMO located close to the center of the NP, whereas the $(TiO_2)_{29}$ truncated NP presents a delocalized SOMO but with contributions mostly at the surface region, and the $(TiO_2)_{43}$ spherical NP bears a SOMO highly localized around the surface region. Thus, since these two factors would, in principle, operate in an opposite way concerning the photocatalytic activity, it is not easy to anticipate which NPs will be more active. It is worth noting that the faceted $(TiO_2)_{35}$ and $(TiO_2)_{29}$ NPs have similar TAS spectra also close to that previously reported for the $(TiO_2)_{38}$ NP,[25] indicating that the latter has notorious structural similarities with the NP models reported here. Furthermore, available experimental TAS experiments for crystalline TiO_2 nanoparticles feature absorption spectra of the trapped holes and electrons with maximum absorption at ca. 520 and ca. 770 nm, respectively, which match well with our computed spectra.[39]

To obtain further insight on the computed absorption spectra, we discuss the assignment of the optical transitions as predicted from our TDDFT calculations. Tables S1-S6 compile the excited electronic states that show an oscillator strength above 1.0($x10^{-3}$). The main excitations have been tabulated considering the following strategy: (*i*) only one excitation is reported in those states where a single excited electronic state has a contribution larger than 20%; (*ii*) a few excitations are compiled when the corresponding excited electronic states contribute above 10%, but below 20%; and finally, (*iii*) only the largest excitation is compiled for those excited electronic states with contributions below 10%. To clarify the discussion, we just focus on the shiniest

excited states corresponding to oscillator strengths equal to or above $2.0x10^{-3}$. For the bipyramidal negatively charged $(TiO_2)_{35}^-$ NP, the TDDFT results evidence three excitation energies at 715.3, 844.9 and 1148.6 nm with oscillator strengths of 2.2, 2.9, and 3.1 ($x10^{-3}$), respectively (Table S1); whereas, in the positively charged $(TiO_2)_{35}^+$ one, the excitation energies at 376.4, 404.5 and 385.8 nm show oscillator strengths of 7.0, 3.4 and 2.0 ($x10^{-3}$), respectively (Table S2). The electronic excitations in the truncated $(TiO_2)_{29}$ NP is more complex (Figure 3). For the negatively charged $(TiO_2)_{29}^-$ a set of six excitations with energies at 544.4, 591.5, 672.5, 706.4, 835.3 and 895.1 nm are relevant with oscillator strengths of 2.0, 2.9, 4.2, 5.7, 7.2 and 3.2 ($x10^{-3}$), respectively (Table S3). On the other hand, for the positively charged $(TiO_2)_{29}^+$ the relevant excitation energies appear at 279.8, 284.0, 291.9, 345.6, 395.8, 471.5, 495.3, and 507 nm with oscillator strengths of 4.1, 2.3, 4.5, 2.1, 4.7, 3.4, 8.0, and 6.8 ($x10^{-3}$), respectively (Table S4). Finally, for the spherical $(TiO_2)_{43}$ NP the absorption spectra of the charged species display a clear overlap (Figure 3) directly reflected in the electronic excitations. The negatively charged $(TiO_2)_{43}^-$ has excitations energies at 302.8, 310.1, 315.6, 323.8, 327.9, 392.9, 421.2, 459.2, and 768.5 nm with oscillator strengths of 7.8, 11.0, 2.8, 3.7, 2.7, 2.5, 5.1, 2.8, and 7.2 ($x10^{-3}$), respectively (Table S5), and the positively charged $(TiO_2)_{43}^+$ shows excitations at 296.0, 360.0, and 376.5 nm with corresponding oscillator strengths of 3.0, 5.6, and 2.1 ($x10^{-3}$), respectively (Table S6). From this analysis one can conclude that the nanoparticle morphology has a negligible influence on the excitations of $(TiO_2)_n^+$ whereas those of $(TiO_2)_n^-$ move towards low wavelength (or high energies) when going to the spherical-shaped morphology, as clearly illustrated in Figure 3. The MOs that participate in the electronic excited states with an oscillator strength larger than $2.0(x10^{-3})$ are depicted in Figures S2-S4.

CONCLUSIONS

In summary, state-of-the-art DFT and TDDFT calculations with the hybrid PBE0 functional have been used to investigate the effect of the nanoparticle morphology on the character of the charged carriers over a selection of TiO_2 NPs covering bipyramidal, truncated and spherical shapes. The computed absorption spectra clearly show that the nanoparticle morphology affects significantly the location of the band and, consequently, the reactivity of the charged carriers. This study shows that the electron charge carriers are particularly sensitive to the morphology, inducing a hypsochromic effect. These electron charge carriers are shallowly trapped in faceted nanoparticles and deeply trapped in spherical ones.

It is expected that the present results constitute a useful input to experimentalists, providing an unbiased alternative way to identify the peaks obtained from the TAS technique. Although our study focuses on titania nanoparticles, similar studies can be performed to analyze the excited states in systems of interest in photocatalysis such as ZnO or WO_3 nanoparticles.

ASSOCIATED CONTENT

The Supporting Information is available free of charge at

Tables S1-S6 compiles the electronic excitations; Figure S1 shows the unrelaxed and relaxed SOMO and SUMO orbitals; Figures S2-S4 show the most relevant MOs involved in the electronic excitations listed in Tables S1-S6.

AUTHOR INFORMATION

Corresponding Author: Ángel Morales-García

E-mail: angel.morales@ub.edu

Notes

The authors declare no competing financial interest.

ACKNOWLEDGMENTS

The research reported in this work has been supported by the Spanish MICIUN RTI2018-095460-B-I00 and *María de Maeztu* MDM-2017-0767 grants, and, in part, by Generalitat de Catalunya 2017SGR13 grant and COST Action CA18234. A. M.-G. thanks to Spanish MICIUN for a *Juan de la Cierva* postdoctoral grant (IJCI-2017-31979) and F. I. acknowledges additional support from the 2015 ICREA Academia Award for Excellence in University Research.

Figure 1. $(TiO_2)_n$ (n = 29, 35, and 43) nanoparticles with truncated, bipyramidal and spherical-like shapes, respectively. Red and gray spheres represent O and Ti atoms, respectively. Bipyramidal $(TiO_2)_{35}$ NP feature only (101) facets, whereas the truncated $(TiO_2)_{29}$ one exhibit both (101) and (001) facets. Note also that the shell of the spherical $(TiO_2)_{43}$ NP is amorphous. Further details about these nanoparticles can be found in refs. 17,19.

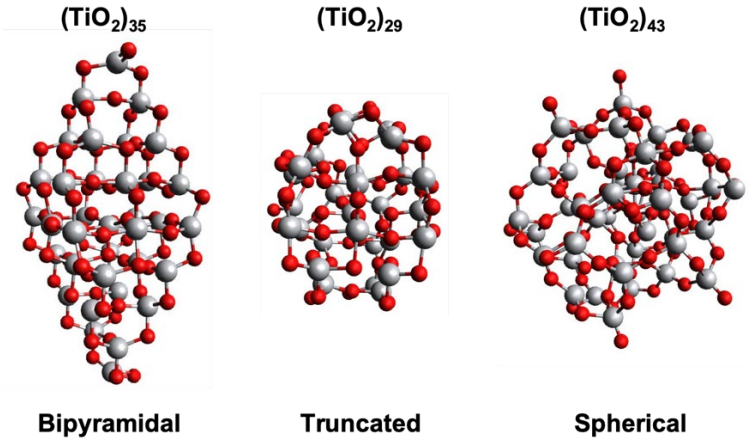

Figure 2. Kohn-Sham energy levels for the $(TiO_2)_{35}$, $(TiO_2)_{29}$, and $(TiO_2)_{43}$ NPs (left, middle, and right, respectively) in the ground, anionic, and cationic states in their unrelaxed and relaxed geometries, calculated at the PBE0/6-31G* level. SUMO and SOMO spinorbitals at the neutral and ionic optimized geometry are depicted in Figure S1 in the Supporting Information.

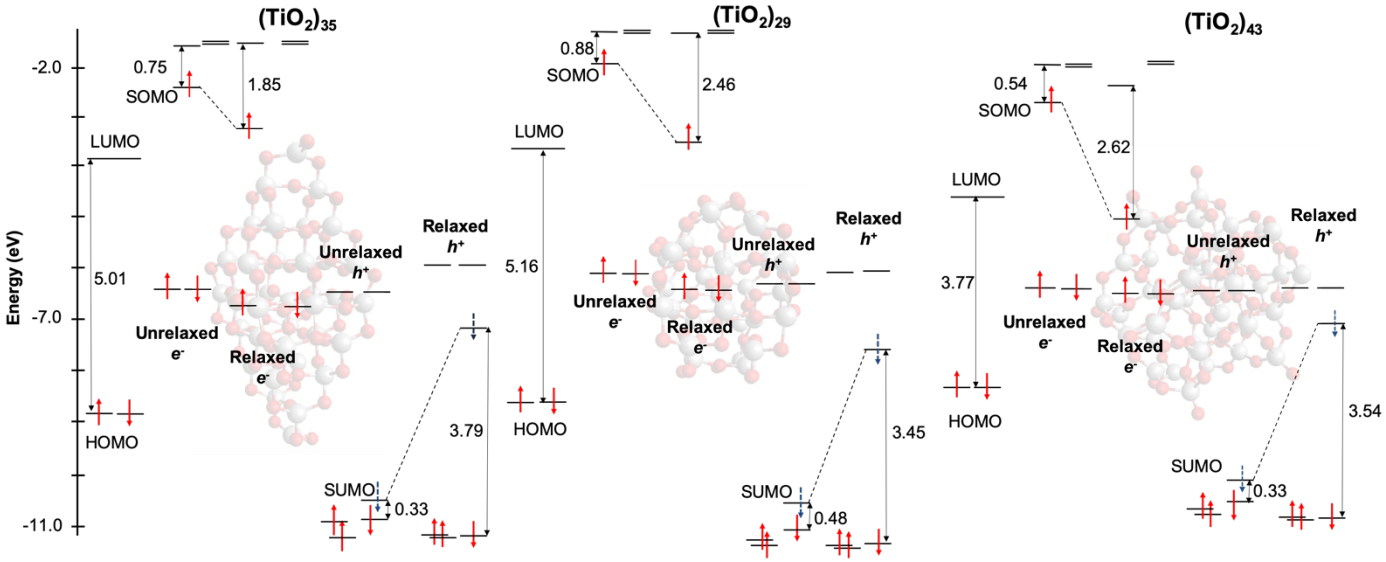

Figure 3. Computed absorption spectra of the $(TiO_2)_n^-$ and $(TiO_2)_n^+$ (n = 29, 35, and 43) NPs, corresponding to an excess electron and excess hole depicted by solid red and light blue lines, respectively, in the relaxed geometries. The solid black line is the sum of the trapped electron and hole contributions.

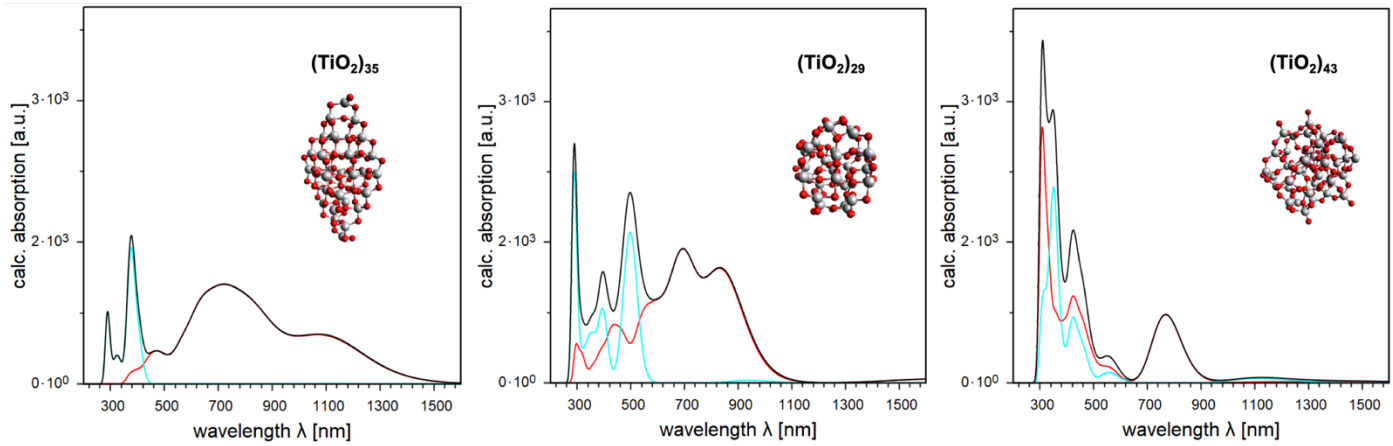

REFERENCES

(1) Fujishima, A.; Honda, K. Electrochemical Photolysis of Water at a Semiconductor Electrode. *Nature* **1972**, *238*, 37-38.

(2) Hoffmann, M. R.; Martin, S. T.; Martin S. T.; Choi, W.; Bahnemann, D. W. Environmental Applications of Semiconductor Photocatalysis. *Chem. Rev.* **1995**, *95*, 69-96.

(3) Ibhadon, A. O.; Fitzpatrick, P. Heterogeneous Photocatalysis: Recent Advances and Applications. *Catalysts* **2013**, *3*, 189-218.

(4) Ahmad, H.; Kamarudin, S. K.; Minggu, L. J.; Kassim, M. Hydrogen from Photo-Catalytic Water Splitting Process: A Review. *Renew. Sust. Energ. Rev.* **2015**, *43*, 599-610.

(5) Mills, A.; Le Hunte, S. An Overview of Semiconductors Photocatalysis. *J. Photoch. Photobio. A* **1997**, *108*, 1-35.

(6) Shneider, J.; Matsuoka, M.; Takeuchi, M.; Zhang, J.; Horiuchi, Y.; Anpo, M.; Bahnemann, D. W. Understanding TiO_2 Photocatalysis: Mechanisms and Materials. *Chem. Rev.* **2014**, *114*, 9919-9986.

(7) De Angelis, F.; Di Valentin, C.; Fantacci, S.; Vittadini, A.; Selloni, A. Theoretical Studies on Anatase and Less Common TiO_2 Phases: Bulk, Surfaces and Nanomaterials. *Chem. Rev.* **2014**, *114*, 9708-9753.

(8) Takanabe, K. Photocatalytic Water Splitting: Quantitative Approaches Toward Photocatalyst by Design. *ACS Catal.* **2017**, *7*, 8006-8022.

(9) Berena, R.; van Grondelle, R.; Kennis, J. T. M. Ultrafast Transient Absorption Spectroscopy: Principles and Applications to Photosynthetic Systems. *Photosynth. Res.* **2009**, *101*, 105-118.

(10) Bahnemann, D.; Henglein, A.; Lilie, J.; Spanbel, L. Flash Photolysis Observation of the Absorption Spectra of Trapped Positive Holes and Electrons in Colloidal TiO_2. *J. Phys. Chem.* **1984**, *88*, 709-711.

(11) Koelle, U.; Moser, J.; Graetzel, M. Dynamics of Interfacial Charge-Transfer Reactions in Semiconductor Dispersions. Reduction of Cobalceniumcarboxylate in Colloidal Titania. *Inorg. Chem.* **1985**, *24*, 2253-2258.

(12) Cho, D.; Ko, K. C.; Lamiel.García, O.; Bromley, S: T.; Lee, J. Y.; Illas, F. Effect of Size and Structure on the Ground-State and Excited-State Electronic Structure of TiO_2 Nanoparticles. *J. Chem. Theory Comput.* **2016**, *12*, 3751-3763.

(13) Di Valentin, C.; Pacchioni, G. Spectroscopic Properties of Doped and Defective Semiconducting Oxides from Hybrid Density Functional Calculations. *Acc. Chem. Res.* **2014**, *47*, 3233-3241.

(14) Tosoni, S.; Lamiel-García, O.; Fernández-Hevia, D.; Doña, J. M.; Illas, F. Electronic Structure of F-doped Bulk Rutile, Anatse and Brookite Polymorphs of TiO_2. *J. Phys. Chem. C* **2012**, *116*, 12738-12746.

(15) Gong, X. Q.; Selloni, A. Reactivity of Anatase TiO_2 Nanoparticles: The Role of the Minority (001) Surfaces. *J. Phys. Chem. B* **2005**, *109*, 19560-19562.

(16) Auvinen, S.; Alatalo, M.; Haario, H.; Jalava, J. P.; Lamminmäki, R. J. Size and Shape Dependence of the Electronic and Spectral Properties in TiO_2 Nanoparticles. *J. Phys. Chem. C* **2011**, *115*, 8484-8493.

(17) Lamiel-García, O.; Ko, K. C.; Lee, J. Y.; Bromley, S. T.; Illas, F. When Anatase Nanoparticles Become Bulklike: Properties of Realistic TiO_2 Nanoparticles in the 1-6 nm Size Range from All Electron Relativistic Density Functional Theory Based Calculations. *J. Chem. Theory Comput.* **2017**, *13*, 1785-1793.

(18) Lamiel-García, O.; Cuko, A.; Calatayud, M.; Illas, F.; Bromley, S. T. Predicting Size-Dependent Emergence of Crystallinity in Nanomaterials: Titania Nanoclusters *versus* Nanocrystals. *Nanoscale* **2017**, *9*, 1049-1058.

(19) Morales-García. Á.; Macià Escatllar, A.; Illas, F.; Bromley, S. T. Understanding the Interplay between Size, Morphology and Energy Gap in Photoactive TiO_2 Nanoparticles. *Nanoscale* **2019**, *11*, 9032-9041.

(20) Wang, X.; Kafikas, A.; Li, X.; Moniz, S. J. A.; Reardon, P. J. T.; Tang, J.; Parkin, I. P.; Durrant, J. R, Transient Absorption Spectroscopy of Anatase and Rutile: The Impact of Morphology and Phase on Photocatalytic Activity. *J. Phys. Chem. C* **2015**, *119*, 10439-10447.

(21) Yamakata, A.; Vequizo, J. J. M.; Matsunaga, H. Distinctive Behavior of Photogenerated Electrons and Holes in Anatase and Rutile TiO_2 Powders. *J. Phys. Chem. C* **2015**, *119*, 24538-24545.

(22) Yang, X. J.; Tamai, N. How Fast is Interfacial Hole Transfer? In Situ Monitoring of Carrier Dynamics in Anatase TiO_2 Nanoparticles by Femtosecond Laser Spectroscopy. *Phys. Chem. Chem. Phys.* **2001**, *3*, 3393-3398.

(23) Bahnemann, D. W.; Hilgendorff, M.; Memming, R. Charge Carrier Dynamics at TiO_2 Particles: Reactivity of Free and Trapped Holes. *J. Phys. Chem. B* **1997**, *101*, 4265-4275.

(24) Cheng, J.; VandeVondele, J.; Sprik, M. Identifying Trapped Electronic Holes at the Aqueous TiO_2 Interface. *J. Phys. Chem. C* **2014**, *118*, 5437-5444.

(25) Nunzi, F.; De Angelis, F.; Selloni, A. Ab Initio Simulation of the Absorption Spectra of Photoexcited Carriers in TiO_2 Nanoparticles. *J. Phys. Chem. Lett.* **2016**, *7*, 3597-3602.

(26) TURBOMOLE V7.3 2018, a development of University of Karlsruhe and Forschungszentrum Karlsruhe GmbH, 1989-2007, TURBOMOLE GmbH, since 2007; available from www.turbomole.com.

([27]) Treutler, O.; Ahlrichs, R. Efficient Molecular Numerical Integration Schemes. *J. Chem. Phys.* **1995**, *102*, 346.

([28]) Eichkorn, K.; Weigend, F.; Treutler, O.; Ahlrichs, R. Auxiliary basis sets for main row atoms and transition metals and their use to approximate Coulomb potentials. *Theor. Chem. Acc.* **1997**, *97*, 119-124.

([29]) Eichkorn, K.; Treutler, O.; Öhm, H.; Häser, M.; Ahlrichs, R. Auxiliary Basis Sets to Approximate Coulomb Potentials. *Chem. Phys. Lett.* **1995**, *242*, 282-290.

([30]) Ahlrichs, R. Efficient evaluation of three-center two-electron integrals over Gaussian functions. *Phys. Chem. Chem. Phys.* **2004**, *6*, 5119-5121.

([31]) Bauernschmitt, R.; Häser, M.; Treutler, O.; Ahlrichs, R. Calculation of excitation energies within time-dependent density functional theory using auxiliary basis set expansions. *Chem. Phys. Lett.* **1997**, *264*, 573-578.

([32]) Weigend, F. Accurate Coulomb-fitting basis sets for H to Rn. *Phys. Chem. Chem. Phys.* **2006**, *8*, 1057-1065.

(33) Nunzi, F.; Agrawal, S.; Selloni, A.; De Angelis, F. Structural and Electronic Properties of Photoexcited TiO_2 Nanoparticles from First Principles. *J. Chem. Theory and Comput.* **2015**, *11*, 635-645.

([34]) Bruhn, T; Schaumlöffel, A.; Hemberger, Y.; Pecitelli, G. SpecDis version 1.71, Berlin, Germany, 2017, https:/specdis-software.jimdo.com.

([35]) Jmol: an open-source Java viewer for chemical structures in 3D. http://www.jmol.org/

(36) Morales-García, Á.; Valero, R.; Illas, F. Reliable and Computationally Affordable Prediction of the Energy Gap of $(TiO_2)_n$ ($10 \leq n \leq 563$) Nanoparticles from Density Functional Theory. *Phys. Chem. Chem. Phys.* **2018**, *20*, 18907-18911.

(37) Katoh, R.; Murai, M.; Furube, A. Transient Absorption Spectra of Nanocrystalline TiO_2 Films at High Excitation Density. *Chem. Phys. Lett.* **2010**, *500*, 309-312.

(38) Tamaki, Y.; Hara, K.; Katoh, R.; Tachiya, M.; Furube, A. Femtosecond Visible-to-IR Spectroscopy of TiO_2 Nanocrystalline Films: Elucidation of the Electron Mobility before Deep Trapping. *J. Phys. Chem. C* **2009**, *113*, 11741-11746.

(39) Yoshihara, T.; Katoh, R.; Furube, A.; Tamaki, Y.; Murai, M.; Hara, K.; Murata, S.; Arakawa, H.; Tachiya, M. Identification of Reactive Species in Photoexcited Nanocrystalline TiO_2 Films by Wide-Wavelength-Range (400-2500 nm) Transient Absorption Spectroscopy. *J. Phys. Chem. B* **2004**, *108*, 3817-3823.

TOC